Research report

Abnormal structural connectivity between the basal ganglia, thalamus, and frontal cortex in patients with disorders of consciousness

Ling Weng [a,1], Qiuyou Xie [b,1], Ling Zhao [a,1], Ruibin Zhang [c], Qing Ma [b], Junjing Wang [a], Wenjie Jiang [a], Yanbin He [b], Yan Chen [b], Changhong Li [a], Xiaoxiao Ni [b], Qin Xu [a], Ronghao Yu [b,**] and Ruiwang Huang [a,*]

[a] Center for the Study of Applied Psychology, Guangdong Key Laboratory of Mental Health and Cognitive Science, School of Psychology, Institute of Brain Science and Rehabilitation, South China Normal University, Guangzhou 510631, PR China
[b] Centre for Hyperbaric Oxygen and Neurorehabilitation, Guangzhou General Hospital of Guangzhou Military Command, Guangzhou 510010, PR China
[c] Department of Psychology, The University of Hong Kong, Hong Kong, PR China

ARTICLE INFO

ABSTRACT

Consciousness loss in patients with severe brain injuries is associated with reduced functional connectivity of the default mode network (DMN), fronto-parietal network, and thalamo-cortical network. However, it is still unclear if the brain white matter connectivity between the above mentioned networks is changed in patients with disorders of consciousness (DOC). In this study, we collected diffusion tensor imaging (DTI) data from 13 patients and 17 healthy controls, constructed whole-brain white matter (WM) structural networks with probabilistic tractography. Afterward, we estimated and compared topological properties, and revealed an altered structural organization in the patients. We found a disturbance in the normal balance between segregation and integration in brain structural networks and detected significantly decreased nodal centralities primarily in the basal ganglia and thalamus in the patients. A network-based statistical analysis detected a subnetwork with uniformly significantly decreased structural connections between the basal ganglia, thalamus, and frontal cortex in the patients. Further analysis indicated that along the WM fiber tracts linking the basal ganglia, thalamus, and frontal cortex, the fractional anisotropy was decreased and the radial diffusivity was increased in the patients compared to the controls. Finally, using the receiver operating characteristic method, we

found that the structural connections within the NBS-derived component that showed differences between the groups demonstrated high sensitivity and specificity (>90%). Our results suggested that major consciousness deficits in DOC patients may be related to the altered WM connections between the basal ganglia, thalamus, and frontal cortex.

1. Introduction

Disorders of consciousness (DOC), which exhibit different levels of dissolution of consciousness including coma, vegetative state/unresponsive wakefulness syndrome (VS/UWS), and minimally conscious state (MCS), have attracted considerable attention from various fields of study and have, therefore, advanced our knowledge of consciousness (Fernandez-Espejo & Owen, 2013; Giacino, Fins, Laureys, & Schiff, 2014; Gosseries, Di, Laureys, & Boly, 2014; Koch, Massimini, Boly, & Tononi, 2016). However, because consciousness is not a unitary construct but a catch-all term that includes wakefulness, awareness, and other phenomena (MacDonald, Naci, MacDonald, & Owen, 2015; Shadlen & Kiani, 2011, pp. 27–46), we still lack an understanding of the neural basis of consciousness. This may block the precise diagnosis of DOC (Steven Laureys & Tononi, 2011). Using non-invasive neuroimaging technology to explore the brain functional and structural alterations in DOC may enable researchers to identify precise diagnostic markers (Owen, 2013; Stender et al., 2014).

A growing number of neuroimaging studies suggest that DOC is a disconnection syndrome (Fernandez-Espejo et al., 2012). For example, Laureys et al. (1999) used Positron Emission Eomography (PET) to reveal functional disconnections in the cortico-cortical and cortico-thalamo-cortical pathways in VS/UWS patients. And resting-state fMRI (R-fMRI) studies showed that the consciousness loss is associated with disrupted functional connections primarily in the default mode network (DMN) (Fernandez-Espejo et al., 2012; Monti et al., 2010), fronto-parietal network (Long et al., 2016), and thalamo-cortical network (Cauda et al., 2009; Crone et al., 2015; Boly et al., 2009). Moreover, several studies indicated that the recovery of consciousness depends to some extent on connectivity between the thalamus and the frontal cortex and parietal regions (Crone et al., 2014; Laureys & Schiff, 2012). A task fMRI study reported that thalamo-frontal connectivity mediates top-down cognitive functions in DOC patients and identified thalamo-frontal connectivity as a neurophysiologic marker that may distinguish patients who can engage in top-down processing from patients who cannot (Monti et al., 2015). Recently, Demertzi et al. (2015) investigated the DMN, fronto-parietal, salience, auditory, sensorimotor and visual networks based on multi-center R-fMRI data (73 DOC patients) by using a multiple-seed correlation approach, and found that the regions in the auditory network were more functionally connected in MCS compared to VS/UWS. Di Perri, Bastianello, and Barrtsch (2013) studied brain functional connectivity between the DMN and other networks in 18 DOC patients, and found the limbic hyperconnectivity in VS/UWS and MCS patients. Annen et al. (2016) studied brain function

(fluorodeoxyglucose FDG-PET metabolism)-structure (DTI) relationship in 25 severely brain injured patients (19 DOC: 7 VS/UWS and 12 MCS; 6 EMCS), and detected regional metabolism was declined in inferior-parietal, precuneus, and frontal regions, as well as abnormal fractional anisotropy (FA) in the thalamo-frontal tracts. To understand the underlying forebrain dysfunction and interventions in severe brain injuries, Schiff (2008, 2010) proposed the "mesocircuit" hypothesis, consisting of striatum, thalamus, frontal cortex, and parietal/occipital/temporal cortex, which provides the conceptual foundation for the key role of the central thalamus as a privileged node for neuromodulation to support forebrain arousal regulation or for a causative role of connectivity from the central thalamus to different cortical areas in DOC patients (Schiff, 2008, 2010, 2016; Giacino et al., 2014). And some studies have tested the "mesocircuit" hypothesis on the basis of R-fMRI connectivity (Lant, Gonzalez-Lara, Owen, & Fernández-Espejo, 2016) and FDG-PET technique (Chatelle et al., 2014; Fridman, Beattie, Broft, Laureys, & Schiff, 2014). Considering that the functional disconnection of the thalamo-frontal circuit may originate from pathological white matter (WM) connectivity and that the thalamo-cortical network plays a role in the cortico-basal ganglia (BG) circuit (Draganski et al., 2008), we attempted to know if the brain WM structural disconnection exists between the BG, thalamus, and frontal cortex in DOC patients.

Diffusion tensor imaging (DTI) is the only available non-invasive technique for detecting the distribution of brain WM *in vivo* (Le Bihan & Johansen-Berg, 2012). It can provide valuable information about WM microstructure and the WM injury severity in DOC patients (Galanaud et al., 2012; Luyt et al., 2012). Fernandez-Espejo et al. (2011) used DTI to study the degrees of axonal injury and damage to the thalami and brainstem regions in 25 VS/UWS and MCS patients by using DTI data. They found significantly different mean diffusivity (MD) value in subcortical white matter and thalamic regions, but not in brainstem, between VS/UWS and MCS patients. And Edlow et al. (2013) mapped brain WM pathways in a post-mortem brain (a 62 years-old woman) with acute traumatic coma by using high angular resolution diffusion imaging (HARDI) data, and found the disrupted WM pathways connecting brainstem arousal nuclei to the basal forebrain and thalamic intralaminar and reticular nuclei. They proposed that traumatic coma may be a subcortical disconnection syndrome related to the disconnection of specific brainstem arousal nuclei from the thalamus and basal forebrain. van der Eerden et al. (2014) reported that DOC patients by Hypoxic Ischemic Encephalopathy (HIE) showed a predominant cerebral hemisphere axonal injury accompanied by a markedly decreased axial diffusivity (AD). Lant et al. (2016) found that DOC patients showed lower FA in the subcortico-cortical and

cortico-cortical fiber tracts than controls. Zheng, Reggente, Lutkenhoff, Owen, and Monti (2017) employed probabilistic tractography in a sample of 25 DOC patients to analyze WM connectivity in thalamo-cortical circuits. They found VS/UWS patients had lower connectivity in most thalamo-cortical circuits, including frontal, temporal, and sensorimotor connections compared to MCS+, and MCS- exhibited significantly less thalamo-premotor and thalamo-temporal connectivity than MCS+. Although most of previous studies analyzed the mylion axonal distribution according to the hypothesis of brain WM disruption in DOC, nearly no study has directly characterized the topological properties of brain axonal fiber profiles in DOC patients *per se*.

A network model, termed the 'connectome' (Hagmann, 2005; Sporns, Tononi, & Kotter, 2005), has been widely used to study various disconnection syndromes caused by brain injury (Catani & ffytche, 2005; Sporns, 2011), including DOC patients (Demertzi et al., 2015; Wu et al., 2015). It conceptualizes the whole-brain as an interconnected network consisting of nodes and edges (Bullmore & Sporns, 2009; Hagmann et al., 2008). The nodes represent brain gray matter (GM) areas, while the edges represent the functional connectivity or structural connectivity between the nodes. In general, structural connectivity corresponds to the WM tracts between pairs of brain GM areas (Rubinov & Sporns, 2010), and mapping the brain structural network has potentially important implications for understanding brain disorders (Crossley et al., 2014; van den Heuvel & Sporns, 2013). Although several DTI analyzed the abnormal topological properties in traumatic brain injury (TBI) patients by analyzing the whole-brain networks (Caeyenberghs et al., 2012; Fagerholm, Hellyer, Scott, Leech, & Sharp, 2015), very few studies explored alterations in the topological properties of brain WM structural networks in DOC patients.

To explore alterations in the brain structural networks in the DOC patients, we first constructed whole-brain WM structural networks and estimated the topological properties for each subject. Then we used a non-parametric permutation test to determine significant changes in topological parameters and used a network based statistic (NBS) approach to test the changes in WM connectivity (Zalesky, Fornito, & Bullmore, 2010) in the DOC patients compared to the healthy control (HC) group. Subsequently, we analyzed the WM connectivity between the BG, thalamus, and frontal cortex that may have originated from WM structural disconnection by comparing between-group differences in the diffusion metrics of several WM tracts: the bilateral anterior and posterior limbs of the internal capsules and the bilateral superior, anterior, and posterior corona radiata. Finally, we explored whether the topological properties that showed group differences could be used to identify the patients with DOC by analyzing the receiver operating characteristic (ROC) curve of the network parameters.

2. Materials and methods

2.1. Subjects

Thirty-five patients with severe brain injuries were recruited from the Coma Recovery Unit of the Center for Hyperbaric Oxygen and Neurorehabilitation in Guangzhou General Hospital of Guangzhou Military Command, from September 2012 to March 2015. Each patient underwent a comprehensive clinical evaluation to estimate the clinical severity of their condition using the Coma Recovery Scale-Revised (CRS-R) (Giacino, Kalmar, & Whyte, 2004; Jones & Cercignani, 2010) three times by 2–3 medical doctors (examiners) in order to make evaluation reliable, (i) a day before the MRI scanning, (ii) on the day of but prior to scanning, and (iii) 1–2 days after the scanning. For each of the patients, we took the best CRS-R scores observed among the three times, which are listed in Table 1. The inclusion criteria for the patients were as follows: 1) disease course less than one year, 2) no history of psychological disorders, 3) no previous alcohol or drug abuse, 4) without epilepsy or frequent spontaneous movements, 5) without the use of the benzodiazepine class of drugs, and 6) no moderate or severe hydrocephalus. All the patients were right-handed according to their

Table 1 — Details of the clinical characteristics and scores on the CRS-R for the 13 DOC patients used in this study. The clinical characteristics and scores on the CRS-R for the other 22 excluded DOC patients are listed in the Supplementary Materials.

Index	Patient	Gender/Age (year old)	Etiology	Intervening weeks (Time since injury)	CRS-R (Auditory/Visual/Motor/Oromotor/Communication/Arousal)	Total CRS-R score
1	VS/UWS 1	M/43	HIE	3	0/0/1/1/0/2	4
2	VS/UWS 2	M/30	TBI	10	1/0/1/1/0/2	5
3	VS/UWS 3	F/27	HIE	3	1/0/1/1/0/2	5
4	VS/UWS 4	M/32	HIE	40	1/0/1/1/0/2	5
5	VS/UWS 5	F/56	HIE	5	1/0/1/1/0/2	5
6	VS/UWS 6	M/39	HIE	3	0/0/2/1/0/2	5
7	MCS 1	F/15	HIE	4	1/3/5/1/0/2	12
8	MCS 2	M/41	TBI	6	1/0/3/1/0/2	7
9	MCS 3	M/17	TBI	10	1/3/2/2/0/2	10
10	MCS 4	M/25	HIE	6	1/3/5/1/0/2	12
11	MCS 5	M/41	HIE	5	2/3/2/1/0/1	9
12	MCS 6	M/34	HIE	6	1/1/5/1/0/2	10
13	MCS 7	F/20	TBI	9	2/3/3/1/0/2	11

Abbreviations: MCS, Minimally Conscious State; VS/UWS, Vegetative State/Unresponsive Wakefulness Syndrome; HIE, Hypoxic Ischemic Encephalopathy; TBI, Traumatic Brain Injury; CRS-R, Coma Recovery Scale-Revised. Intervening weeks: No. of weeks since ictus or time since injury.

guardians' reports. In addition, we also recruited 17 gender-, age-, and handedness-matched healthy subjects (8 F/9 M, aged 20-51 years old, age = 33.88 ± 10.43 years old) as the controls. None of the controls had a history of neurological or psychiatric illnesses or brain injuries. The protocols were approved by the Research Review Board of Guangzhou General Hospital of Guangzhou Military Command. Written informed consent was obtained from each healthy subject and from the legal surrogate for each patient.

2.2. Data acquisition

All MRI data were acquired on a 3T GE MRI scanner with an eight-channel phased-array head coil. The DTI data were collected 30 diffusion weighted volumes with $b = 1000$ sec/mm^2 and 3 b_0 volumes using single-shot diffusion-weighted EPI sequence, and T1-weighted brain structural images using 3D fast spoiled gradient recalled (SPGR) sequence. The detailed scanning setting and sequence parameters are described in the Supplementary Materials. To reduce the head motion effect related to voluntary movements common to DOC patients, we acquired DTI data from the DOC patients under sedation (Cavaliere et al., 2014).

2.3. Image quality checking

Because it is not easy to perform co-registration and spatial normalization in DOC patients and it is also quite difficult to obtain adequate segmented images of the WM and CSF for each patient (Lutkenhoff et al., 2014), we visually checked the quality of the diffusion images, the high resolution brain structural images, and the conventional MRI scans for all the subjects, especially for the DOC patients. After carefully visually inspecting the brain images, we excluded 22 patients from the recruited 35 patients for several reasons (Fig. 1). In the end, we retained 13 DOC patients (4 F/9 M, 7MCS/6 VS/UWS, aged 15–56 years, age = 32.31 ± 11.71 years, 4 TBI/9 HIE, brain injury time 3–40 weeks, injury time = 8.46 ± 9.79 weeks) for further analysis. The detailed clinical information for the 13 included DOC patients is listed in Table 1 and for the 22 excluded patients in Supplementary Table S1.

2.4. Data preprocessing

All DTI data were processed with PANDA package (Cui, Zhong, Xu, He, & Gong, 2013) under a Linux Operating System. For each subject, we first preprocessed the diffusion data by following typical approaches, including brain tissue extraction, eddy-current distortion correction by registering the diffusion-weighted images to the b_0 images with an affine transformation, and B-matrix correction (Leemans & Jones, 2009). Then we performed voxel-wise computation for the diffusion tensor and diffusion metrics, FA, MD, AD, and radial diffusivity (RD). The detailed processing steps are described in the Supplementary Materials.
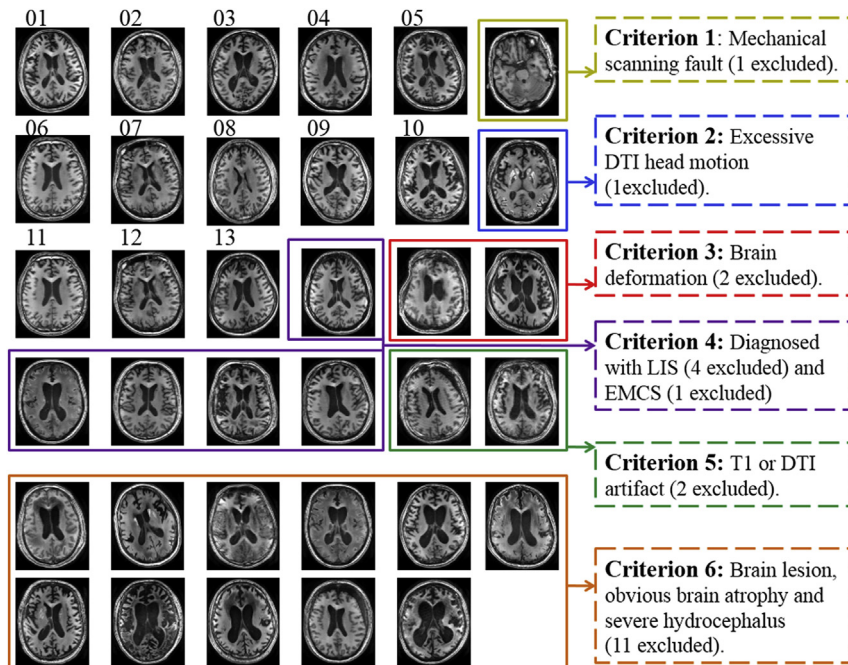
Fig. 1 – **The pipeline for checking the brain images of the DOC patients. High resolution T1-weighted 3D brain structural images for all of the 35 patients with severe brain injuries in this study are presented here. As shown in the figure, we excluded 22 DTI datasets from the 35 patients with severe brain injuries due to a mechanical scanning fault that led to bad image quality (1 subject) or due to excessive head motion (1 subject), brain deformation (2 subjects), or T1-weighted or artifacts (2 subjects), or because the patents were diagnosed with LIS (locked-in syndrome) or EMCS (emerged minimally conscious state) (5 subjects), or with brain lesions, obvious brain atrophy, or severe hydrocephalus (11 subjects). In the end, 13 DOC patients, numbered in this paper from 01 to 13, were included for further group analysis in this study.**

2.5. Network construction

2.5.1. Node definition

The human brain structural network for each subject was constructed according to the automated anatomical labeling (AAL) atlas, which parcellates the whole-brain into 90 (45 for each hemisphere) cortical and subcortical regions of interest (ROIs). The names and abbreviations of these ROIs are listed in Supplementary Table S3. Each ROI represented a node of the brain network and the connectivity between each pair of ROIs constituted an edge.

2.5.2. Edge weight definition and connectivity probability

We reconstructed the whole-brain WM tracts using a probabilistic tractographic method (Behrens, Berg, Jbabdi, Rushworth, & Woolrich, 2007). We selected each ROI of the AAL-90 atlas as a seed region and used the other 89 ROIs as the target regions to perform the probabilistic tractography, repeating this process for all the ROIs. Given two ROIs, the connectivity probability from region i to region j, p_{ij}, was defined as the number of fibers passing through the target region j divided by the total of $5{,}000 \times n$ fibers, where n is the total number of voxels in the seed region i. Notably, the connectivity probability from region i to region j, p_{ij}, is not necessarily equivalent to the probability from region j to region i, p_{ji}, because the tractography is dependent on the seeding location. We defined the unidirectional connectivity probability between regions i and j by averaging these two probabilities,

$$P_{ij} = \left(p_{ij} + p_{ji}\right)\big/2. \tag{1}$$

Next, we took the averaged connectivity probability as the edge weight between regions i and j in the brain network. In this way, we constructed a 90×90 symmetric weighted matrix to represent the weighted brain WM network for each subject. The work-flow for the construction of the network is shown in Supplementary Fig. 1.

2.6. Network analysis

2.6.1. Network threshold selection

To avoid the biases associated with using a single threshold, we examined the topological properties using a range of thresholds. Specifically, two ROIs were considered connected if the mean connectivity probability across all the subjects in this study was more than 2 standard deviations (SDs) above a given threshold, i. e.,

$$\text{mean } (P_{ij}) > \text{threshold} + 2*\text{SD}(P_{ij}), \tag{2}$$

otherwise, these two ROIs were considered unconnected (Cao et al., 2013; Gong et al., 2009). Following previous studies (Draganski et al., 2008; Gong et al., 2009), we set the minimal threshold value at $P_{ij} = .01$ to remove spurious connections and set the maximum threshold value at $P_{ij} = .05$ to maintain the average size of the largest connected component at approximately 90 across all the subjects. Finally, we set threshold values for the connectivity probability ranging from $P_{ij} = .01$ to .05 at intervals of $\Delta P_{ij} = .0025$ to analyze the network topological properties. Under these thresholds, the corresponding network sparsities ranged from 4.5% to 8.9%.

2.6.2. Network parameters

We characterized the global topological properties of the brain WM structural networks by using seven parameters: clustering coefficient (C_p), characteristic path length (L_p), global efficiency (E_{glob}), local efficiency (E_{loc}), normalized clustering coefficient (γ), normalized characteristic path length (λ), and small-worldness (σ). Additionally, we used nodal efficiency and nodal degree to characterize the nodal topology of the brain networks. We use the probability of inter-regional connectivity as the edge weight to define and calculate the network parameters. The definitions and interpretations for these global and nodal parameters are listed in Supplementary Table S2 and can also be found in Rubinov and Sporns (2010).

In order to compare between-group differences in the topological organization, we calculated the area under the curve (AUC) for each network metric over a range of thresholds from $P_{ij} = .01-.05$ at intervals of $\Delta P_{ij} = .0025$. This yielded 17 corresponding connectivity matrices for each subject. As suggested by previous studies (Cao et al., 2013; Gong et al., 2009), the AUC portrays the topological organization of brain networks in a summarized scalar that is independent of any single threshold selection. All the network analyses were performed using the GRETNA toolbox (Wang et al., 2015).

2.7. WM connections analysis

Using a NBS approach (Zalesky, Fornito, & Bullmore, 2010), we identified any connected subnetwork in which each of the WM connections was significantly changed in the DOC patients compared to the HCs. In the calculations, we set the significance level of $p < .05$ (corrected for multiple comparisons). Before the analysis, we removed the effects of age, gender, and the total motion index (TMI) on the between-group differences in the connections before performing the statistical analysis. A detailed description of the NBS is described in the Supplementary Materials as well as in Zalesky, Fornito, and Bullmore (2010).

2.8. Diffusion metrics alteration in WM tracts

A tract-wise analysis of the diffusion metrics was also performed for the brain WM fiber tracts, which were extracted according to the ICBM-DTI-81 WM labels atlas (Mori et al., 2008). The bilateral superior, anterior, and posterior corona radiata as well as the bilateral anterior and posterior limbs of the internal capsules connect the BG, thalamus, and frontal cortex. We compared between-group differences in the diffusion metrics (e.g., FA, MD, AD, and RD) of these WM fiber tracts. The values of the AD and RD respectively represent the diffusivity of water molecules in directions perpendicular to or parallel to the principal axis of diffusion in anisotropic regions of brain WM (Jones, Knosche, & Turner, 2013).

2.9. Statistical analysis

2.9.1. Between-group comparison

We used a χ^2-test to assess the difference in gender and a two-sample t-test to analyze the difference in age between the two groups. A nonparametric permutation t-test was used to

determine the significant between-group differences in the AUC value of the network parameters and to perform a tract-wise fiber analysis (10,000 permutations, see details in the Supplementary materials). Before the permutation test, we regressed out the confounding effects of age, gender, and TMI. For the network parameters with significant between-group differences, we also estimated their effect size (Cohen's *d*) (Cohen, 1992).

2.9.2. Correlations between the NBS-derived component and diffusion metrics

For the acquired significant NBS component, we further calculated the correlation between the component strength and the diffusion metrics of the bilateral anterior and posterior limb of the internal capsule and the bilateral superior, anterior, and posterior corona radiata. The NBS-derived component strength was defined as the average connectivity strength of all the connections that were contained in the component. We performed a multiple linear regression analysis by taking the NBS-derived component strength as a dependent variable and the diffusion metrics as independent variables. In the calculations, we treated age, gender, and TMI as confounding covariates.

2.9.3. Correlations between network and clinical parameters

For those network parameters with significant between-group differences, we further assessed the relationship between any of these parameters and the CRS-R total score across all the DOC patients. We performed a multiple linear regression analysis by taking the network parameters as dependent variables and the CRS-R total score as the independent variable. In the calculations, we treated age, gender, and TMI as confounding covariates.

2.10. ROC curve

Identifying reorganized brain networks in DOC patients may provide clues for predicting their recovery (Chennu et al., 2014; Silva et al., 2015). For the network parameters that showed significant between-group differences, we plotted the ROC curve to determine which of these parameters could clearly distinguish the DOC from the HC. The ROC curve, which is widely used in medical science, is a fundamental plot in signal detection theory (Desco, Hernandez, Santos, & Brammer, 2001; Pencina, D'Agostino, D'Agostino, & Vasan, 2008). A ROC, a scatter plot showing the relationship between false alarm rates and hit rates, describes the relationship between the underlying distribution of the places where signals are absent and the places where signals are present. This analysis was performed using public MATLAB codes (http://www.mathworks.com/matlabcentral/fileexchange/199500-roc-curve; by Giuseppe Cardillo).

2.11. Robustness analysis

The robustness of network parameters is a key issue in network analysis (Telesford, Burdette, & Laurienti, 2013) and a connectivity-based parcellation methods was used to define ROIs in neuroimaging research (Eickhoff, Thirion, Varoquaux, & Bzdok, 2015). To test the robustness of our

findings obtained using our primary strategy (nodes defined from AAL-90), we repeated the network analysis by defining the nodes according to another parcellation template, the Harvard-Oxford Atlas (HOA-110) (Caviness, Meyer, Makris, & Kennedy, 1996).

2.12. Cross-validation

The cross-validation was performed by repeating the same analysis while adopting a leave-one-dataset-out cross-validation (LODO-CV) approach (Duff et al., 2015; Schurger, Pereira, Treisman, & Cohen, 2010) in which one patient's data was removed from all of the DTI datasets to find out if the results would remain significant. The rationale of this test is that if a previous significant result remains in all or most of the combinations of subjects, we may conclude that the finding is highly replicable. In this study, we excluded one DOC patient at a time from the DOC group and thus had 13 combinations of subjects.

3. Results

3.1. Demographic information and head motion measures

Table 2 shows that we found no significant between-group differences in either gender ($p = .37$, χ^2-test) or age ($p = .70$, two-sample *t*-test). We also found that the head motion measures of the included 13 DOC patients were not significantly different from the 17 HCs: translation ($p = .17$, two-sample *t*-test) and rotation ($p = .20$, two-sample *t*-test). The other 2 head motion measures, the drop-out severity and the portion of slices with drop-out equaled 1 and 0, respectively, for all the subjects (Supplementary Fig. S2).

Table 2 − Demographic and clinical details of the patients with disorders of consciousness (DOC) and the healthy controls (HC) in this study.

Characteristics	DOC	HC	*p*-value
	(*n* = 13)	(*n* = 17)	
Gender (Male/Female)	9/4	9/8	.37[a]
Age (years old)	32.31 ± 11.71	33.88 ± 10.43	.70[b]
Diagnosis (MCS, VS/UWS)	7/6	N/A	N/A
Etiology: HIE/TBI	9/4	N/A	N/A
CRS-R Score	7.69 ± 3.04	N/A	N/A
Translation of DTI scan (mm)	.59 ± .26	.48 ± .10	.17[b]
Rotation of DTI scan (degree)	.005 ± .003	.004 ± .001	.20[b]

We used the TMI (total motion index) to represent the head motion values for each subject.
Abbreviations: MCS, Minimally Conscious State; VS/UWS, Vegetative State/Unresponsive Wakefulness Syndrome; HIE, Hypoxic Ischemic Encephalopathy; TBI, Traumatic Brain Injury; CRS-R, Coma Recovery Scale-Revised. N/A, not applicable.
[a] *p*-value was obtained using the χ^2-test.
[b] *p*-value was obtained using the two-sample two-tailed *t*-test.

3.2. Global properties

We found the structural networks for both the DOC patients and HCs satisfied the criteria for small-world organization in the connectivity probability range of $P_{ij} = .01-.05$ (Fig. 2A). Compared to the controls, the DOC patients showed a significantly decreased AUC value for E_{loc} ($p = .006$) and C_p ($p = .042$). Marginally significant between-group differences in the AUC values were detected in either L_p ($p = .051$) or E_{glob} ($p = .098$). In addition, we detected a significantly decreased C_p and significantly increased L_p at several values of the probability threshold in the patients compared to the controls (Fig. 2B). Fig. 2B shows the plots of the other global parameters (C_p, L_p, E_{loc}, and E_{glob}) as they changed with the threshold of the probabilistic connectivity. The inserted bar plots indicate the AUC values of these global parameters for both groups.

3.3. Nodal properties

Fig. 3 shows the abnormal brain regions in the patients that had significant between-group differences in their nodal centralities ($p < .05$, FDR corrected). Compared to the controls, the patients showed uniformly significantly decreased nodal efficiency in nine brain regions, as listed in Table 3. Of these, eight were located in the BG system (bilateral caudate, bilateral putamen, bilateral pallidum, and bilateral thalamus) along with a region, the left amygdala. We also found that the patients showed a uniformly significantly decreased nodal degree in fifteen brain regions compared to the controls (Table 3). Interestingly, eight regions with decreased nodal efficiency also showed significantly decreased nodal degree in the patients (Fig. 3 and Table 3). The other seven brain regions with decreased nodal degree in the DOC patients were located in the left frontal cortex (the left precentral gyrus, PreCG.L; left dorsolateral superior frontal gyrus, SFGdor.L), parietal cortex (right angular gyrus, ANG.R; left inferior parietal gyrus, IPL.L), and occipital cortex (right middle occipital gyrus, MOG.R; bilateral inferior occipital gyri, IOG.L/R).

3.4. Decreased WM connections in the DOC

Fig. 4 shows the NBS-derived subnetwork, in which the patients had uniformly significantly decreased inter-regional WM connections compared to the controls ($p = .002$, FWE corrected). This subnetwork consisted of 21 connections between 20 ROIs. Of the 21 connections, seven abnormal connections were related to the BG and thalamus; another nine linked the frontal regions, BG, and thalamus; four more were located within the frontal cortex; and the last one abnormal connection linked the frontal and parietal cortices. The connectivity strength of each connection within the NBS-derived subnetwork is listed in Table 4.

3.5. Diffusion metrics alterations in WM tracts

Fig. 5A shows the WM fiber tracts that were selected for performing the tract-wise analysis of the diffusion metrics between the two groups. We found a statistically significant
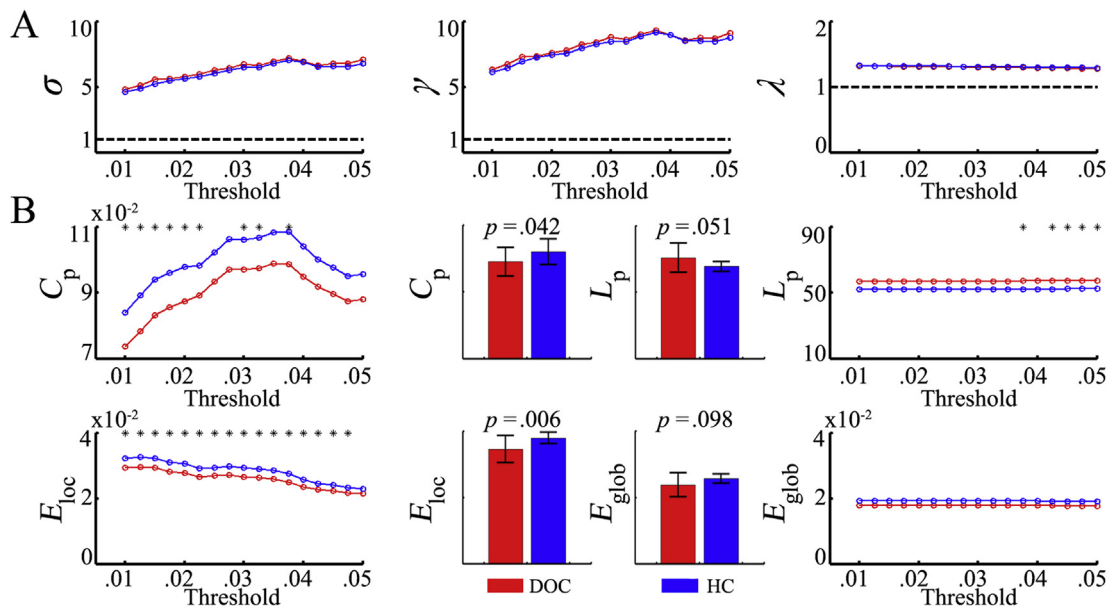

Fig. 2 — Global topological parameters of the brain white matter structural networks showing the change in the parameters at different thresholds of probabilistic connectivity (ranging from .01 to .05, at intervals of .0025) in the DOC patients and the healthy controls (HC). (A) The small-worldness properties of the DOC patients and controls. The dashed line represents a value of 1. The value of $\sigma > 1$, or $\gamma >> 1$ and $\lambda \approx 1$, indicates that the brain structural networks for both groups showed small-world properties at all thresholds. (B) The other four global topological parameters. The * indicates significant between-group differences in the given global parameter at the specific threshold ($p < .05$, permutation test). The inserted bar plot indicates between-group comparisons of the area under the curve (AUC) for the given parameter. The bar height represents the group averaged AUC value and the error bar represents the standard deviation of the AUC across the subject group. Abbreviations: σ, small-worldness; γ, normalized clustering coefficient; λ, normalized characteristic path length; C_p, clustering coefficient; L_p, characteristic path length; E_{loc}, local efficiency; E_{glob}, global efficiency.
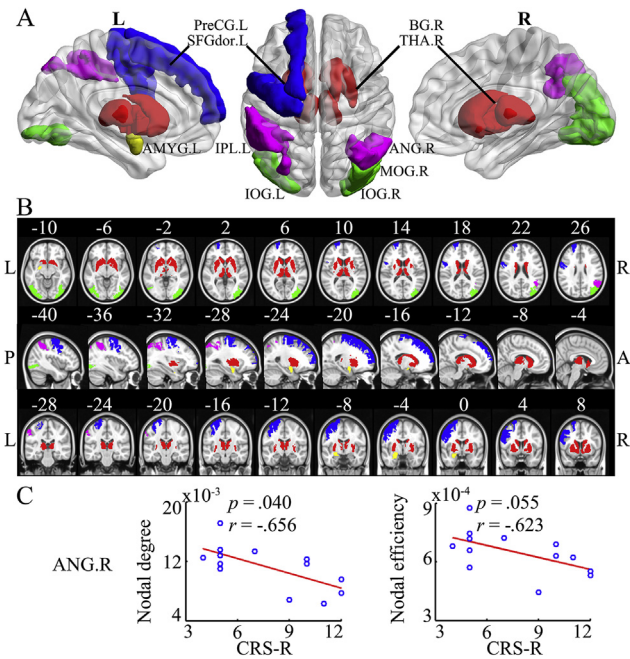
Fig. 3 — Brain regions showing abnormal nodal centralities (nodal efficiency and degree) in the DOC patients compared to the healthy controls (HC). (A) Rendering plot of abnormal brain regions in the DOC patients on the ICBM-152 surface using BrainNet Viewer software (http://www.nitrc.org/projects/bnv/). Red: BG and thalamus; Blue: frontal cortex; Green: occipital cortex; Yellow: temporal region; Violet: parietal region. (B) Axial, sagittal, and coronal views of the abnormal brain regions on the MNI152 space (using MRIcroN software http://www.nitrc.org/projects/mricron/). The color-coding for the different regions is the same as that used above. (C) Scatter plots of the nodal parameters against the total score on the CRS-R across all the DOC patients. The nodal − degree were significantly (p < .05) correlated with the CRS-R scale in the DOC patients only for the right angular gyrus. The abbreviations for the brain regions are presented in Tables 3 and 4.

lower average FA (p = 1.00e-4) and higher average MD (p = 1.00e-4) for the tracts in the DOC patients than in the controls (Fig. 5B). Further analyses revealed significantly increased average RD values (p = 1.00e-4) but no difference in the average AD (p = .24) in these tracts of the DOC patients compared to the HC (Fig. 5B).

3.6. Relationship between network parameters and clinical variables

No significant correlation was found between the network parameters (C_p, L_p, E_{loc}, and E_{glob}) and the CRS-R total score in the DOC patients or between the mean values of the component strength within the NBS-derived subnetwork and the CRS-R total score. However, in the ANG.R, the nodal degree was significantly negatively correlated (r = −.656, p = .040) with the CRS-R total score and the nodal efficiency was marginally significantly negatively correlated (r = −.623, p = .055) with the CRS-R total score (Fig. 3C). The p-values for

the relationship between network parameters and clinical variables were not corrected for multiple comparisons.

3.7. ROC curve

Table 5 lists the differentiation rate derived from the ROC analysis for each of these network parameters (nodal efficiency, nodal degree, and NBS-derived network). Of the metrics with good classification accuracy, the component strength of the NBS-derived subnetwork that had significantly decreased connections had the greatest ability to distinguish the DOC patients from the controls (AUC = .993; sensitivity = 1.000; specificity = 1.000; efficiency = 1.000; p < 1.00e-4) (Fig. 4C).

3.8. Cross-validation

As seen in Table 5, the LODO-CV showed that the reported between-group differences in this study were highly replicable or were almost completely preserved in the 13 combinations of subjects.

3.9. Robustness analysis

Another brain parcellation, HOA-110, also found small-worldness in both the DOC patients and the controls. The direction of the changes in the network parameters (C_p, L_p, E_{glob}, E_{loc}) for the HOA-110 was the same as for the AAL-90, although the nodes that showed significantly decreased nodal efficiency differed from those for the AAL-90 (Supplementary Fig. S3 and Table S4).

4. Discussion

Using graph theory and the NBS approach, we studied the topological organization of brain WM networks constructed using diffusion probabilistic tractography in DOC patients. At the global level, we found that the DOC patients showed significantly decreased clustering coefficient and local efficiency as well as marginally increased characteristic path length. At the nodal level, we found that the DOC patients showed significantly decreased nodal efficiency and degree primarily in the BG, the thalamus, and the frontal regions compared to the controls. Moreover, the NBS analysis revealed significantly decreased structural connectivity between the BG, the thalamus, and the frontal cortex in the DOC patients. The decreased component strengths of NBS in the DOC patients may arise from the changes of underlying WM tissue microstructure, such as myelin and axonal density, as indicated by decreased FA in the bilateral anterior and posterior limbs of the internal capsules and the bilateral superior, anterior, and posterior corona radiate (Beaulieu, 2002; Wheeler-Kingshott & Cercignani, 2009).

4.1. Altered global integration and local specialization in the patients

In this study, we found that both the DOC patients and the healthy controls showed small-worldness in their brain WM

Table 3 − **Brain regions with significantly decreased nodal centralities (nodal efficiency, nodal degree) in the DOC patients compared to the healthy controls (HC). The* and bold font indicate significant between-group difference ($p < .05$, FDR corrected) in the corresponding nodal parameter.**

Index	Brain regions	Nodal efficiency			Nodal degree		
		DOC (*1e-4)	HC (*1e-4)	p-value (effect size)	DOC (*1e-3)	HC (*1e-3)	p-value (effect size)
	BG system						
1	Caudate.L	6.18	7.20	**2.0e-4* (1.0)**	6.83	9.54	**1.0e-4* (1.0)**
2	Caudate.R	6.09	6.79	**6.0e-4* (.9)**	7.03	8.88	**1.0e-4* (1.0)**
3	Putamen.L	7.02	8.10	**2.0e-4* (1.0)**	14.39	17.55	**1.0e-4* (1.0)**
4	Putamen.R	7.12	7.89	**1.5e-3* (.9)**	15.21	16.91	**2.2e-3* (.8)**
5	Pallidum.L	6.33	7.34	**1.0e-4* (1.0)**	8.33	10.31	**1.0e-4* (1.0)**
6	Pallidum.R	6.40	7.10	**9.0e-4* (.9)**	8.77	9.83	2.0e-2 (.5)
7	Thalamus.L	4.49	5.99	**1.0e-4* (1.0)**	3.11	5.96	**1.0e-4* (1.0)**
8	Thalamus.R	4.62	6.19	**1.0e-4* (1.0)**	3.53	6.80	**1.0e-4* (1.0)**
	Frontal						
9	PreCG.L	7.03	7.78	2.7e-2 (.5)	11.78	13.67	**2.0e-3* (.9)**
10	SFGdor.L	7.31	8.24	2.5e-2 (.5)	11.37	13.48	**3.8e-3* (.8)**
	Occipital						
11	MOG.R	6.85	7.79	4.3e-2 (.4)	8.99	12.08	**3.0e-4* (.9)**
12	IOG.L	6.58	7.43	3.0e-2 (.4)	9.50	11.59	**8.2e-3* (.7)**
13	IOG.R	5.66	6.36	3.4e-2 (.5)	6.94	8.68	**2.5e-3* (.8)**
	Temporal						
14	AMYG.L	5.89	6.87	**4.0e-4* (1.0)**	10.26	12.79	**5.0e-4* (1.0)**
	Parietal						
15	ANG.R	6.50	7.46	9.3e-3 (.7)	11.28	14.26	**4.9e-3* (.8)**
16	IPL.L	7.97	8.71	1.3e-1 (.2)	15.39	17.67	**8.4e-3* (.7)**

Abbreviation: BG, Basal ganglia. BG system here consists of bilateral caudate, putamen, pallidum, and thalamus. IOG, inferior occipital gyrus; MOG, middle occipital gyrus; PreCG, precentral gyrus; SFGdor, dorsolateral of superior frontal gyrus; AMYG, amygdala; ANG, angular gyrus; IPL, inferior parietal gyrus, L (R), left (right) hemisphere. The effect size was calculated by using Cohen's d. The small, medium, and large levels of the effect size are .2, .5, .8 respectively, according to Cohen's definition (Cohen, 1992).

networks (Fig. 2A). This result is in line with previous studies (Caeyenberghs et al., 2012; Crone et al., 2014). The small-worldness topology reflects an optimal balance between global integration, which is supported by the characteristic path length and local specialization, which is supported by local efficiency (Sporns, Tononi, & Edelman, 2000). Such a balance is essential for the high level functioning of human brain networks (Honey & Sporns, 2008). Our findings of significantly decreased clustering coefficient, local efficiency and a tendency toward increased characteristic path length in the DOC patients (Fig. 2B) may indicate a great disturbance between segregation and integration in brain structural networks. This disturbance may lead to deficits and fluctuations in cognitive functioning in DOC patients (Crone et al., 2014).

4.2. Altered nodal parameters in the thalamus and frontal regions in the patients

Our study detected significantly decreased nodal efficiency and nodal degree in the bilateral thalamus in the DOC patients compared to the controls (Fig. 3 and Table 3). This finding may reflect impaired structure in the thalamus. The thalamus is known to play a key role in arousal regulation and the support of human consciousness (Schiff, 2008). Direct widespread thalamic injuries can produce persistent disturbances of consciousness in terms of goal-directed behavior and communication skills (Schiff & Plum, 2000). Schiff and Fins (2007) showed that bilateral deep brain electrical stimulation (DBS) of the central thalamus can modulate and improve

behavioral responsiveness in a patient who had remained in a MCS for 6 years following a TBI. Lutkenhoff et al. (2015) used T1-weighted brain structural MR images from a sample of 143 DOC patients to assess structural atrophy in the bilateral thalamus, BG, hippocampus, basal forebrain, and brainstem. They found that the clinical measures of awareness and wakefulness in DOC patients were associated with tissue atrophy within the thalamic and BG nuclei and the non-traumatic injuries exhibited more extensive thalamic atrophy. According to the definitions of the nodal parameters (Supplementary Table S2), the degree value indicates the importance of a node in the network and nodal efficiency indicates the efficiency of information processing and transmission in the brain (Bullmore & Sporns, 2009; Rubinov & Sporns, 2010). Thus, an impaired thalamus may produce severe alterations in brain information integration and may promote deficits in cognitive functioning and conscious processing in DOC patients. Combined with previous findings about brain volume atrophy in the thalamus (Fernandez-Espejo et al., 2010; Lutkenhoff et al., 2015), our results indicated that the impaired levels of nodal properties in the right thalamus may relate to various levels of consciousness deficits and may partially relate to the levels of wakefulness and awareness in VS/UWS and MCS patients.

We found decreased nodal parameters in the frontal cortex (the left precentral gyrus and left dorsolateral superior frontal gyrus) and parietal cortex (the left inferior parietal gyrus), corresponding to the fronto-parietal network (Table 3). The fronto-parietal network is associated with goal-directed
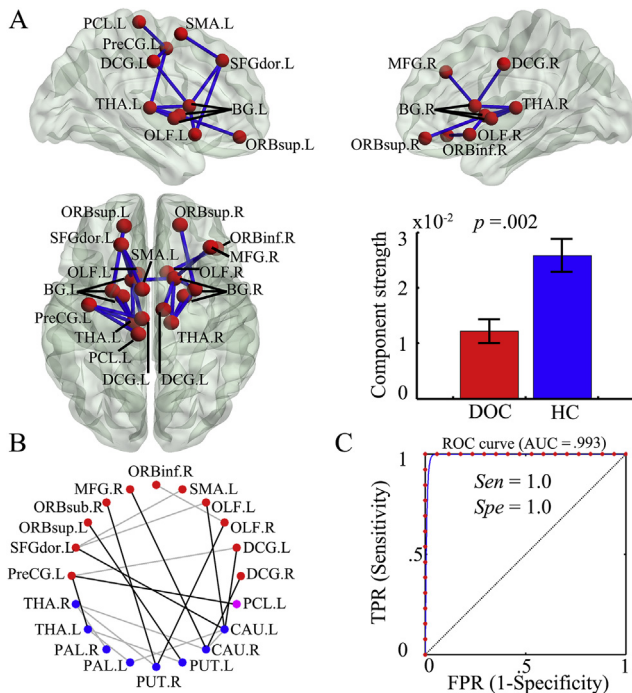
Fig. 4 – The subnetwork derived from the network-based statistic (NBS) analysis showing uniformly significantly decreased connections in the DOC patients compared to the healthy controls (HC). (A) NBS-derived component. The circuit consists of 20 brain regions and 21 connections. The bar height indicates that all 21 connections were significantly decreased ($p = .002$, corrected) in the patients compared to the controls. (B) The altered 21 connections belong to the basal ganglia (BG), thalamus, and frontal cortex. Color-coding: Blue nodes: BG regions and thalamus; Red nodes: frontal regions; Black line (between red and blue nodes): decreased connections between the BG, thalamus, and frontal regions. Grey line: the decreased connection within the BG and thalamus or within the frontal regions. Detailed information is provided in Table 4. (C) The ROC curve based on the structural connections within the NBS-derived component. It shows that the NBS component had a strong ability to discriminate the DOC patients from the HCs (AUC > .9). TPR, true positive rate; FPR, false positive rate; Sen, sensitivity; Spe, specificity; AUC, area under curve. The abbreviations for the brain regions are presented in Tables 3 and 4.

behaviors, cognitive control (Zanto & Gazzaley, 2013), declarative memory retrievals, and updating working memory (Borst & Anderson, 2013). Several studies suggested that impairment in the fronto-parietal network has a severe impact on information integration, which is reflected in deficits in cognitive functioning and probably leads to deficits of consciousness (Cavinato et al., 2015; Crone et al., 2014; Demertzi, Soddu, & Laureys, 2013). For example, using the R-fMRI data, Crone et al. (2014) detected abnormal network properties of the fronto-parietal network in impaired consciousness patients. And Boly et al. (2011) measured effective connectivity in VS/UWS patients during a mismatch negativity paradigm through analyzing long-latency evoked event-

related potential (ERP) components, found that the only significant difference between VS/UWS patients and healthy controls was an impairment of backward connectivity from frontal to temporal cortices, and further revealed significant difference in the backward connectivity between VS/UWS and MCS patients. In practice, previous studies suggested that the fronto-parietal network is involved in working memory (Salazar, Dotson, Bressler, & Gray, 2012), cognitive control (Zanto & Gazzaley, 2013), reasoning ability (Wendelken, Ferrer, Whitaker, & Bunge, 2015), attention, and self-awareness (Ham et al., 2014). Thus, our finding of decreased nodal parameters in the fronto-parietal network may indicate disrupted internal and external awareness in DOC patients.

Previous studies indicated that the middle occipital gyrus (MOG) and inferior occipital gyrus (IOG) play critical roles in the recognition of objects and spatial processing (Ishai, Ungerleider, Martin, & Haxby, 2000; Renier et al., 2010). Actually, previous studies reported that MCS patients show more often visual and motor responses than auditory responses (Bagnato et al., 2016; Estraneo et al., 2015), and visual subscale (along with the auditory one) was responsible for the variability observed in patients with DOC (Cortese et al., 2015). Thus, the significant decreases of nodal parameters in these regions may reflect the abilities of visual processing in the DOC patients are seriously affected.

4.3. Decreased structural connections in the NBS-derived subnetworks of DOC

Using the NBS approach, we identified a subnetwork (Fig. 4) and found decreased subcortico-cortical structural connectivity of the BG and the thalamus with the frontal cortex and of the BG with the thalamus in the DOC patients compared to the controls. We showed that ROC analysis also revealed that brain WM connectivity between subcortico-cortical demonstrated excellent classification accuracy (Fig. 4). Previous studies have pointed out the central role of the circuit of the BG, thalamus, and frontal cortex in the modulation of motor, cognitive, limbic function, and goal-directed behaviors (Draganski et al., 2008; Haber, 2003) and indicated that impaired connectivity in this circuit may have disastrous impacts on consciousness (Boly et al., 2009; Cauda et al., 2009; Cavinato et al., 2015; Crone et al., 2014; Demertzi et al., 2013). Akeju et al. (2015) studied the neural correlate of dexmedetomidine-induced unconsciousness in 10 healthy volunteers with PET and fMRI techniques and found that a loss of thalamo-cortical functional connectivity was sufficient to produce unconsciousness. Monti et al. (2015) analyzed task-fMRI data from 28 DOC patients (8 VS/UWS, 16 MCS, and 4 exit from MCS) using a psychophysiologic interaction (PPI) method and revealed that the thalamo-frontal circuit may be crucial to sustaining top-down cognitive functions in DOC and that disconnectivity in this circuit leads to severe deficits in awareness. We also noticed decreased subcortico-cortical connectivity between the striatum (caudate and putamen), thalamus, and frontal cortex in this subnetwork (Fig. 4B). This result is also in line with the findings reported in two review papers (Schiff, 2008, 2010), which indicated that structural impairment within a cortico-striatopallidal-thalamo-cortical circuit may be key for defining the characteristics of DOC.

Table 4 — Subnetwork composed of uniformly significantly decreased connections in the DOC patients compared to the healthy controls (HC). These connections formed a connected subnetwork identified using a network-based statistic (NBS) approach ($p = .002$, corrected).

Index	Connection	Connectivity strength		t-score	p-value
		DOC ($n = 13$)	HC ($n = 17$)		
		Mean ± SD ($*10^{-2}$)	Mean ± SD ($*10^{-2}$)		
	BG − BG				
1	CAU.L − THA.L	1.26 ± .51	4.98 ± 1.47	9.11	1.00e-04
2	CAU.R − THA.R	1.48 ± .46	4.91 ± 1.56	7.49	1.00e-04
3	PAL.R − THA.R	2.17 ± 1.50	6.03 ± 1.71	6.56	1.00e-04
4	PAL.L − THA.L	1.03 ± .96	3.89 ± 1.52	5.53	1.00e-04
6	PUT.R − THA.R	.19 ± .24	.88 ± .53	4.23	1.00e-04
5	CAU.L − CAU.R	.16 ± .20	.87 ± .55	4.18	1.00e-04
7	PUT.L − THA.L	.18 ± .17	1.07 ± .68	3.99	4.00e-04
	Frontal − BG				
8	DCG.L − CAU.L	.06 ± .08	.74 ± .32	7.51	1.00e-04
9	PreCG.L − THA.L	.08 ± .13	.69 ± .40	5.04	1.00e-04
10	OLF.R − PUT.R	.69 ± .50	1.39 ± .63	4.33	2.00e-04
11	DCG.R − CAU.R	.17 ± .22	.79 ± .46	4.32	3.00e-04
12	ORBsup.R − PUT.R	.80 ± .78	2.08 ± 1.20	3.93	4.00e-04
13	ORBsup.L − PUT.L	.70 ± .74	1.60 ± 1.29	3.88	1.00e-04
14	MFG.R − CAU.R	.57 ± .36	1.32 ± .75	3.51	4.00e-04
15	SFGdor.L − CAU.L	.15 ± .12	.66 ± .50	3.46	9.00e-04
16	OLF.L − CAU.L	7.28 ± 1.05	8.59 ± 1.19	3.29	1.00e-03
	Frontal − Frontal				
17	PreCG.L-DCG.L	.69 ± .36	1.10 ± .30	3.92	4.00e-04
18	SFGdor.L-SMA.L	5.13 ± 1.91	7.22 ± .96	3.78	5.00e-04
19	SFGdor.L-OLF.L	.02 ± .05	.53 ± .54	3.60	8.00e-04
20	ORBinf.R-OLF.R	.90 ± .35	1.64 ± .57	3.58	9.00e-04
	Frontal − Parietal				
21	PreCG.L − PCL.L	1.89 ± .77	3.23 ± .91	4.44	3.00e-04

Abbreviation: BG, Basal ganglia. BG system here consists of the bilateral caudate, putamen, pallidum, and thalamus. CAU, caudate; PUT, putamen; PAL, pallidum; THA, thalamus; DCG, median cingulate and paracingulate gyri; MFG, middle frontal gyrus; OLF, olfactory cortex; ORBinf, orbital part of the inferior frontal gyrus; ORBsup, orbital part of the superior frontal gyrus; PCL, paracentral lobule; PreCG, precental gyrus; SFGdor, superior frontal gyrus, dorsolateral; SMA, supplementary motor area; L (R), left (right) hemisphere. We arranged these connections within the BG system, between the frontal cortex and the BG system, within the frontal cortex, and between the frontal and parietal regions according to their t-scores.

Thus, our current finding from the structural WM connectivity perspective may lay a foundation for the structural basis of the functional disconnectivity in the BG, thalamus, and frontal cortex circuit.

4.4. Diffusion metrics alteration in WM tracts

The bilateral anterior and posterior corona radiata as well as the bilateral anterior and posterior limbs of the internal capsules connect the BG, thalamus, and the frontal cortex. These tract-wise analyses were plotted using the ICBM-DTI-81 WM labels atlas (Fig. 5A). Through analyzing the diffusion metrics, we found a significantly decreased average FA and increased average MD of those tracts in the DOC patients compared to the controls. This finding is consistent with a previous review paper about TBI (Hulkower, Poliak, Rosenbaum, Zimmerman, & Lipton, 2013). Specifically, the reduced FA and increased MD respectively reflect impaired WM integrity and disruption of the WM microstructures (Jones et al., 2013). Also, we further found significantly increased average RD without a changed average AD of those tracts in the DOC patients compared to the controls. This finding is also consistent with several previous studies (Kraus et al., 2007; van der Eerden et al., 2014).

Kraus et al. (2007) identified both axonal damage and myelin damage in severe TBI, and van der Eerden et al. (2014) reported that HIE patients showed a predominant cerebral hemisphere axonal injury accompanied by a markedly decreased AD.

According to the DTI model, RD stands for the profile of the water molecular diffusivity perpendicular to the WM tracts' main direction and AD for the profile of the water molecular diffusivity perpendicular parallel to the WM tracts' main direction. Thus, both AD and RD can be used to assess brain WM microstructure or myelin integrity (Song et al., 2003, 2005). Considering the alterations in the tracts connecting the BG, thalamus, and frontal cortex, we inferred that the damaged WM microstructure in patients may primarily related to the alterations of myelin and axonal density of the brain WM (Beaulieu, 2002; 2013). Notably, van der Eerden et al. (2014) demonstrated that TBI patients chiefly showed central myelin injury accompanied by a marked increase in RD primarily in the brainstem, anterior and posterior limbs of the internal capsule, and corona radiata. This may indicate that deficits in WM microstructure caused the abnormal average RD in the tracts connecting the BG, thalamus, and frontal cortex and then affected the topological organization of the brain structural network in DOC patients.
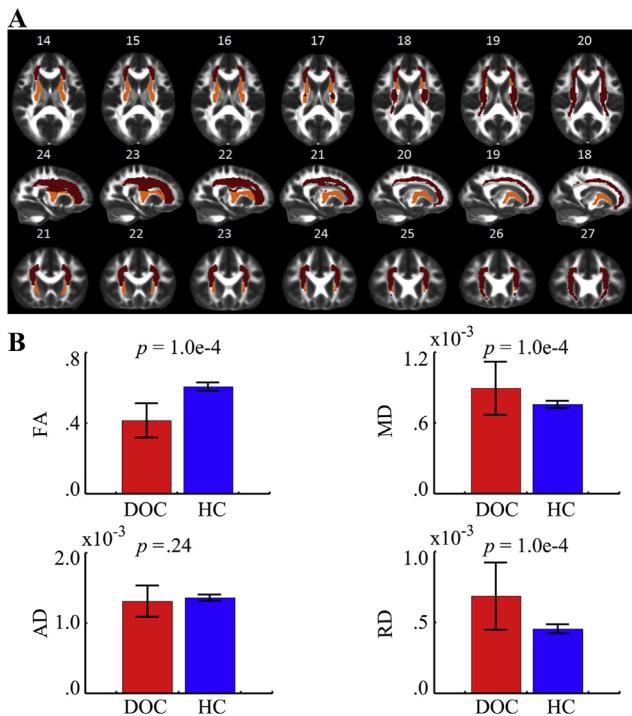
A

B

Fig. 5 − Group differences in the diffusion metrics (FA, MD, AD, and RD) between the DOC patients and the healthy controls (HC). (A) Location of selected tracts using the ICBM_DTI_81 probabilistic white matter atlas and rendering on the FMRIB58_FA template. Color-coding: Dark-red: bilateral superior, anterior, and posterior corona radiata; Orange: bilateral anterior and posterior limb of the internal capsule. (B) The average diffusion metrics value for selected tracts in the DOC patients and the controls.

4.5. Relationship between network parameters and clinical variables

For the regions and inter-regional connections listed in Tables 3 and 4, we estimated correlations between these network parameters and the total CRS-R in the patients. We found only in the ANG.R, the nodal degree was significantly negatively correlated to total CRS-R in the patients (Fig. 3C). Farrer et al. (2008) suggested that the ANG is responsible to process the inconsistency between behavior consequence and awareness of own action authorship. The reduced nodal degree in the right ANG may indicate dysfunction of own authorship in the patients.

4.6. Limitations and strengths

Several limitations need to be addressed. First, DTI data may be sensitive to head motion artifacts or susceptibility or eddy-current distortion (Posnansky, Kupriyanova, & Shah, 2011). To reduce the effect of susceptibility and eddy-current on diffusion-sensitive gradients in fiber tracking, we estimated the modified B-matrix (Leemans & Jones, 2009) and used it in the calculations. To reduce the head motion effect, we acquired DTI data from the DOC patients under sedation, which can, to a certain degree, restrict the artifacts in DTI data

resulting from the involuntary movements common to DOC patients (Cavaliere et al., 2014). We also visually excluded the subjects that had excessive head motion, estimated the head motion measures, and took the TMI (Supplementary Fig. S2) as a covariate in the statistical analysis (Yendiki, Koldewyn, Kakunoori, Kanwisher, & Fischl, 2013). Second, because the brains of DOC patients are more likely to be atrophic than those of healthy controls, normalization is more difficult in DOC patients. For small ROIs, it is often misalignment between b_0 images and diffusion-weighted images, and then leads to imperfect registration to the Montreal Neurological Institute (MNI) space. Even a small error in ROI placement can have a large effect on FA, streamline counts and fiber tracking related to the ROI (van den Heuvel & Sporns, 2011). Though several normalization methods have been proposed (Andersen, Rapcsak, & Beeson, 2010; Lutkenhoff et al., 2014; Ripolles et al., 2012), we found that it was still not easy to get good normalization results in the DOC group. Thus we excluded the patients with larger structural disturbances caused by TBI, cerebral hematomas, or severe widespread cerebral atrophy (Fig. 1). Third, the definitions of the nodes and edge weights may affect the findings obtained from the brain structural networks in DOC patients. Previous studies (de Reus & van den Heuvel, 2013; Zalesky, Fornito, & Bullmore, 2010; Zalesky, Fornito, Harding, et al., 2010; Zhong, He, & Gong, 2015; Proix et al., 2016) have analyzed the effects of definitions of nodes and edge weights, DTI acquisition protocols, and fiber tracking approaches on the topological attributes of whole-brain WM structural networks. Currently, the number of short-range cortico-cortical WM connections is underrepresented in large-scale brain structural networks, and it is still unclear which scale of representation of WM fibers is optimal to describe brain topological property. This means that no definitive way has been developed to select the nodes when constructing brain networks. The lack of a gold standard for constructing brain networks makes the definitions of nodes arbitrary, meaning that network nodes are defined using brain templates either random or predefined brain parcellations. Various brain atlases, such as the AAL-90, AAL-1024, and HOA-110 templates, have been used to define the network nodes (Zhang et al., 2015). In addition, different studies have defined the edge weights as the number of fibers, the mean FA values of the connected fibers, and the weighted fiber density (Andersen et al., 2010; Zhang et al., 2015). In this study, we selected a widely applied template, the AAL-90 template, to define the nodes, and selected the widely adopted connectivity probability to define edge weight, as given in eq. (1). We used the AUC, which is the summarization of the network metrics over a range of thresholds, to perform between-group comparisons. Fourth, we took the best CRS-R scores without considering the score variation in this study. Cortese et al. (2015) indicated that the CRS-R varies with examination time in a day after analyzing the CRS-R repeatedly administered to 7 VS/UWS and 12 MCS patients undergoing systematic observation during a conventional 13 weeks. They found the CRS-R total score, visual and auditory subscores higher (about 30%) in the morning than at the afternoon administration in both VS/UWS and MCS subgroups over the entire period of observation. They advised multiple CRS-R testing is an effective way to minimize the risk of misclassification. Thus, in our

Table 5 — Results of the sensitivity analysis and the receiver operating characteristic (ROC) curve analysis for the network parameters that showed significant between-group differences. We used the leave-one-out approach to determine the cross-validation ratio, which shows the number of times that the reported significant result remained significant in all 13 combinations of subjects.

Parameters	Cross-validation (Ratio)	ROC curve				
		AUC (%)	Sensitivity (%)	Specificity (%)	Efficiency (%)	*p*-value
Global parameter						
C_p	7/13	67.90	46.15	88.24	70.00	.04
E_{loc}	13/13	83.57	76.92	94.12	86.67	<1.00e-04
Nodal efficiency						
AMYG.L	13/13	86.31	92.31	70.59	80.00	<1.00e-04
CAU.L	13/13	93.37	92.31	88.24	90.00	<1.00e-04
CAU.R	13/13	81.90	84.62	82.35	83.33	<1.00e-04
PUT.L	13/13	91.46	84.62	94.12	90.00	<1.00e-04
PUT.R	13/13	83.53	76.92	88.24	83.33	<1.00e-04
PAL.L	13/13	91.19	76.92	94.12	86.67	<1.00e-04
PAL.R	13/13	82.32	69.23	94.12	83.33	<1.00e-04
THA.L	13/13	93.78	100.00	82.35	90.00	<1.00e-04
THA.R	13/13	95.35	100.00	82.35	90.00	<1.00e-04
Nodal degree						
PreCG.L	13/13	82.18	69.23	94.12	83.33	<1.00e-04
SFGdor.L	13/13	80.49	76.92	88.24	83.33	<1.00e-04
AMYG.L	13/13	87.49	92.31	82.35	86.67	<1.00e-04
MOG.R	13/13	86.40	76.92	100.00	90.00	<1.00e-04
IOG.L	13/13	90.32	84.62	100.00	93.33	<1.00e-04
IOG.R	13/13	83.20	84.62	94.12	90.00	<1.00e-04
IPL.L	4/13	85.20	92.31	70.59	80.00	<1.00e-04
ANG.R	9/13	83.91	76.92	88.24	83.33	<1.00e-04
CAU.L	13/13	95.38	92.31	94.12	93.33	<1.00e-04
CAU.R	13/13	94.60	100.00	88.24	93.33	<1.00e-04
PUT.L	13/13	88.73	84.62	88.24	86.67	<1.00e-04
PUT.R	13/13	75.27	61.54	94.12	80.00	3.30e-03
PAL.L	13/13	88.34	84.62	88.24	86.67	<1.00e-04
THA.L	13/13	93.78	92.31	88.24	90.00	<1.00e-04
THA.R	13/13	96.14	84.62	100.00	93.33	<1.00e-04
NBS						
	13/13	99.31	100.00	100.00	100.00	<1.00e-04

Abbreviation: AMYG, amygdala; PreCG, precentral gyrus; SFGdor, dorsolateral of superior frontal gyrus; MOG, middle occipital gyrus; IOG, inferior occipital gyrus; ANG, angular gyrus; IPL, inferior parietal gyrus, L (R), left (right) hemisphere. Other abbreviations see Tables 3 and 4 please.

study, the CRS-R score was evaluated 3 times for each patient by 2–3 examiners in order to make evaluation reliable and we took the best CRS-R scores observed for the patient. And the evaluation of CRS-R scores may depend on the training background and level of experience of examiners. The improbable subscore combinations have been discussed by Chatelle et al. (2016), which analyzed CRS-R subscores in 1,190 DOC patients for detecting inaccurate and unusual scores, and tabulated 9 impossible and 36 improbable subscore combinations based on CRS-R scoring guidelines. Fifth, the sample size of the subjects (13 DOC patients) in this study was small and was selected from a larger sample of 35 patients (Fig. 1). This may affect the generality of the findings. Because our sample size was limited, we estimated the statistical power and effect size and conducted a sensitivity analysis by using a leave-one-dataset-out cross validation. The sensitivity analysis indicated that our findings were highly replicable. We also plotted ROC curves for the network parameters that showed significant between-group differences, and the results revealed a high statistical power and effect size for these

parameters. The ROC curves also showed that the strength of the NBS-derived component with significantly decreased connections had the greatest ability to distinguish the DOCs from the HCs. Fifth, we utilized data from DOC patients, some of whom were TBI and others were HIE patients and thus had differences in their pathogenesis. In future studies a better way would be to classify the patients into different subgroups according to their various etiologies to elucidate how the abnormal structural topology contributes to brain dysfunction in different types of DOC patients (Fernandez-Espejo et al., 2011). Last but not least, although we found the abnormal white matter connections between the basal ganglia, thalamus, and frontal cortex in the patients, we cannot infer if these changes are associated with consequence of the brain injury or impaired consciousness itself. In the future, a longitudinal study, combining the measure of electrophysiological indices of consciousness (Casali et al., 2013) with the indices of brain functional and structural connectivity (Barttfeld et al., 2015), is needed to understand the DOC-related neural mechanism.

5.   Conclusion

To summarize, this study constructed brain WM structural networks in DOC patients based on DTI data and analyzed the topological properties using graph theory. We found that the DOC patients showed reduced structural connections between the BG, thalamus, and frontal cortex, reduced local efficiency, reduced nodal properties in the BG, thalamus, frontal, and occipital regions, as well as reduced structural connectivity in the NBS-derived subnetwork. The diffusion metrics analysis also revealed reduced FA and increased RD in the brain WM of the DOC patients. This suggested that the abnormal structural connectivity in DOC patients may be due to myelin damage in the brain white matter. Finding abnormal connectivity in the BG, thalamus, and frontal cortex revealed the structural basis of the functional disconnection identified in previous fMRI studies using DOC patients. The findings provide useful information for understanding brain WM abnormalities in patients with DOC patients.

Competing interests statement

The authors declare that they have no competing financial interests.

Supplementary data

Supplementary data related to this article can be found at http://dx.doi.org/10.1016/j.cortex.2017.02.011.

R E F E R E N C E S

Akeju, O., Loggia, M. L., Catana, C., Pavone, K. J., Vazquez, R., Rhee, J., et al. (2015). Disruption of thalamic functional connectivity is a neural correlate of dexmedetomidine-induced unconsciousness. eLife, 3, e04499.

Andersen, S. M., Rapcsak, S. Z., & Beeson, P. M. (2010). Cost function masking during normalization of brains with focal lesions: Still a necessity? NeuroImage, 53(1), 78–84. http://dx.doi.org/10.1016/j.neuroimage.2010.06.003.

Annen, J., Heine, L., Ziegler, E., Frasso, G., Bahri, M., Di Perri, C., et al. (2016). Function–structure connectivity in patients with severe brain injury as measured by MRI-DWI and FDG-PET. Human Brain Mapping, 37(11), 3707–3720. http://dx.doi.org/10.1002/hbm.23269.

Bagnato, S., Boccagni, C., Sant'Angelo, A., Fingelkurts, A. A., Fingelkurts, A. A., & Galardi, G. (2016 May). Longitudinal assessment of clinical signs of recovery in patients with unresponsive wakefulness syndrome after traumatic or nontraumatic brain injury. Journal of Neurotrauma. http://dx.doi.org/10.1089/neu.2016.4418 (ahead of print).

Barttfeld, P., Uhrig, L., Sitt, J. D., Sigman, M., Jarraya, B., & Dehaene, S. (2015). Signature of consciousness in the dynamics of resting-state brain activity. Proceedings of the National Academy of Sciences of the United States of America, 112(3), 887–892. http://dx.doi.org/10.1073/pnas.1418031112.

Beaulieu, C. (2002). The basis of anisotropic water diffusion in the nervous system – A technical review. NMR in Biomedicine, 15(7–8), 435–455. http://dx.doi.org/10.1002/nbm.782.

Beaulieu, C. (2013). The biological basis of diffusion anisotropy (Chap. 6). In T. E. J. B. Heidi Johansen-Berg (Ed.), Diffusion MRI: From quantitative measurement to in vivo neuroanatomy (2ed., pp. 1–614). Academic Press is an imprint of Elsevier.

Behrens, T. E., Berg, H. J., Jbabdi, S., Rushworth, M. F., & Woolrich, M. W. (2007). Probabilistic diffusion tractography with multiple fibre orientations: What can we gain? NeuroImage, 34(1), 144–155. http://dx.doi.org/10.1016/j.neuroimage.2006.09.018.

Boly, M., Garrido, M. I., Gosseries, O., Bruno, M. A., Boveroux, P., Schnakers, C., et al. (2011). Preserved feedforward but impaired top-down processes in the vegetative state. Science, 332(6031), 858–862. http://dx.doi.org/10.1126/science.1202043.

Boly, M., Tshibanda, L., Vanhaudenhuyse, A., Noirhomme, Q., Schnakers, C., Ledoux, D., et al. (2009). Functional connectivity in the default network during resting state is preserved in a vegetative but not in a brain dead patient. Human Brain Mapping, 30(8), 2393–2400.

Borst, J. P., & Anderson, J. R. (2013). Using model-based functional MRI to locate working memory updates and declarative memory retrievals in the fronto-parietal network. Proceedings of the National Academy of Sciences of the United States of America, 110(5), 1628–1633.

Bullmore, E., & Sporns, O. (2009). Complex brain networks: Graph theoretical analysis of structural and functional systems. Nature Reviews Neuroscience, 10(3), 186–198. http://dx.doi.org/10.1038/nrn2575.

Caeyenberghs, K., Leemans, A., De Decker, C., Heitger, M., Drijkoningen, D., Linden, C. V., et al. (2012). Brain connectivity and postural control in young traumatic brain injury patients: A diffusion MRI based network analysis. NeuroImage: Clinical, 1(1), 106–115. http://dx.doi.org/10.1016/j.nicl.2012.09.011.

Cao, Q., Shu, N., An, L., Wang, P., Sun, L., Xia, M. R., et al. (2013). Probabilistic diffusion tractography and graph theory analysis reveal abnormal white matter structural connectivity networks in drug-naive boys with attention deficit/hyperactivity disorder. The Journal of Neuroscience, 33(26), 10676–10687. http://dx.doi.org/10.1523/JNEUROSCI.4793-12.2013.

Casali, A. G., Gosseries, O., Rosanova, M., Boly, M., Sarasso, S., Casali, K. R., et al. (2013). A theoretically based index of consciousness independent of sensory processing and behavior. Science Translational Medicine, 5(198). doi: ARTN 198ra105.

Catani, M., & ffytche, D. H. (2005). The rises and falls of disconnection syndromes. Brain, 128(Pt 10), 2224–2239. http://dx.doi.org/10.1093/brain/awh622.

Cauda, F., Micon, B., Sacco, K., Duca, S., D'Agata, F., Geminiani, G., et al. (2009). Disrupted intrinsic functional connectivity in the vegetative state. Journal of Neurology, Neurosurgery, and Psychiatry, 80(4), 429–431.

Cavaliere, C., Aiello, M., Di Perri, C., Fernandez-Espejo, D., Owen, A. M., & Soddu, A. (2014). Diffusion tensor imaging and white matter abnormalities in patients with disorders of

consciousness. *Frontiers in Human Neuroscience, 8*, 1028. http://dx.doi.org/10.3389/fnhum.2014.01028.

Cavinato, M., Genna, C., Manganotti, P., Formaggio, E., Storti, S. F., Campostrini, S., et al. (2015). Coherence and consciousness: Study of fronto-parietal gamma synchrony in patients with disorders of consciousness. *Brain Topography, 28*(4), 570–579. http://dx.doi.org/10.1007/s10548-014-0383-5.

Caviness, V. S., Jr., Meyer, J., Makris, N., & Kennedy, D. N. (1996). MRI-based topographic parcellation of human neocortex: An anatomically specified method with estimate of reliability. *Journal of Cognitive Neuroscience, 8*(6), 566–587. http://dx.doi.org/10.1162/jocn.1996.8.6.566.

Chatelle, C., Bodien, Y. G., Carlowicz, C., Wannez, S., Charland-Verville, V., Gosseries, O., et al. (2016). Detection and interpretation of impossible and improbable coma recovery scale-revised scores. *Archives of Physical Medicine and Rehabilitation, 97*(8), 1295–1300. http://dx.doi.org/10.1016/j.apmr.2016.02.009. e1294.

Chatelle, C., Thibaut, A., Gosseries, O., Bruno, M. A., Demertzi, A., Bernard, C., et al. (2014). Changes in cerebral metabolism in patients with a minimally conscious state responding to zolpidem. *Frontiers in Human Neuroscience, 8*, 917. http://dx.doi.org/10.3389/fnhum.2014.00917.

Chennu, S., Finoia, P., Kamau, E., Allanson, J., Williams, G. B., Monti, M. M., et al. (2014). Spectral signatures of reorganised brain networks in disorders of consciousness. *Plos Computational Biology, 10*(10), e1003887. http://dx.doi.org/10.1371/journal.pcbi.1003887.

Cohen, J. (1992). A power primer. *Psychological Bulletin, 112*(1), 155–159.

Cortese, M., Riganello, F., Arcuri, F., Pugliese, M., Lucca, L., Dolce, G., et al. (2015). Coma recovery scale-r: Variability in the disorder of consciousness [journal article] *BMC Neurology, 15*(1), 1–7. http://dx.doi.org/10.1186/s12883-015-0455-5.

Crone, J. S., Schurz, M., Höller, Y., Bergmann, J., Monti, M., Schmid, E., et al. (2015). Impaired consciousness is linked to changes in effective connectivity of the posterior cingulate cortex within the default mode network. *NeuroImage, 110*, 101–109.

Crone, J. S., Soddu, A., Höller, Y., Vanhaudenhuyse, A., Schurz, M., Bergmann, J., et al. (2014). Altered network properties of the fronto-parietal network and the thalamus in impaired consciousness. *NeuroImage: Clinical, 4*, 240–248.

Crossley, N. A., Mechelli, A., Scott, J., Carletti, F., Fox, P. T., McGuire, P., et al. (2014). The hubs of the human connectome are generally implicated in the anatomy of brain disorders. *Brain, 137*, 2382–2395. http://dx.doi.org/10.1093/Brain/Awu132.

Cui, Z., Zhong, S., Xu, P., He, Y., & Gong, G. (2013). PANDA: A pipeline toolbox for analyzing brain diffusion images. *Frontiers in Human Neuroscience, 7*, 42. http://dx.doi.org/10.3389/fnhum.2013.00042.

Demertzi, A., Antonopoulos, G., Heine, L., Voss, H. U., Crone, J. S., de Los Angeles, C., et al. (2015). Intrinsic functional connectivity differentiates minimally conscious from unresponsive patients. *Brain, 138*(Pt 9), 2619–2631. http://dx.doi.org/10.1093/brain/awv169.

Demertzi, A., Soddu, A., & Laureys, S. (2013). Consciousness supporting networks. *Current Opinion in Neurobiology, 23*(2), 239–244. http://dx.doi.org/10.1016/j.conb.2012.12.003.

Desco, M., Hernandez, J. A., Santos, A., & Brammer, M. (2001). Multiresolution analysis in fMRI: Sensitivity and specificity in the detection of brain activation. *Human Brain Mapping, 14*(1), 16–27.

Di Perri, C., Bastianello, S., & Barrtsch, A. J. (2013). Limbic hyperactivity in the vegetative state. *Neurology, 81*(16), 1417–1424. http://dx.doi.org/10.1212/WNL.0b013e3182a43b78.

Draganski, B., Kherif, F., Kloppel, S., Cook, P. A., Alexander, D. C., Parker, G. J., et al. (2008). Evidence for segregated and integrative connectivity patterns in the human Basal Ganglia.

The Journal of Neuroscience, 28(28), 7143–7152. http://dx.doi.org/10.1523/JNEUROSCI.1486-08.2008.

Duff, E. P., Vennart, W., Wise, R. G., Howard, M. A., Harris, R. E., Lee, M., et al. (2015). Learning to identify CNS drug action and efficacy using multistudy fMRI data. *Science Translational Medicine, 7*(274), 274ra216-274ra216.

Edlow, B. L., Haynes, R. L., Takahashi, E., Klein, J. P., Cummings, P., Benner, T., et al. (2013). Disconnection of the Ascending Arousal System in Traumatic Coma. *Journal of Neuropathology & Experimental Neurology, 72*(6), 505–523.

van der Eerden, A. W., Khalilzadeh, O., Perlbarg, V., Dinkel, J., Sanchez, P., Vos, P. E., et al. (2014). White matter changes in comatose survivors of anoxic ischemic encephalopathy and traumatic brain injury: Comparative diffusion-tensor imaging study. *Radiology, 270*(2), 506–516. http://dx.doi.org/10.1148/radiol.13122720.

Eickhoff, S. B., Thirion, B., Varoquaux, G., & Bzdok, D. (2015). Connectivity-based parcellation: Critique and implications. *Human Brain Mapping, 36*(12), 4771–4792. http://dx.doi.org/10.1002/hbm.22933.

Estraneo, A., Moretta, P., Cardinale, V., De, T. A., Gatta, G., Giacino, J. T., et al. (2015). A multicentre study of intentional behavioural responses measured using the Coma Recovery Scale-Revised in patients with minimally conscious state. *Clinical Rehabilitation, 29*(8), 803.

Fagerholm, E. D., Hellyer, P. J., Scott, G., Leech, R., & Sharp, D. J. (2015). Disconnection of network hubs and cognitive impairment after traumatic brain injury. *Brain, 138*(Pt 6), 1696–1709. http://dx.doi.org/10.1093/brain/awv075.

Farrer, C., Frey, S. H., Van Horn, J. D., Tunik, E., Turk, D., Inati, S., et al. (2008). The angular gyrus computes action awareness representations. *Cerebral Cortex, 18*(2), 254–261.

Fernandez-Espejo, D., Bekinschtein, T., Monti, M. M., Pickard, J. D., Junque, C., Coleman, M. R., et al. (2011). Diffusion weighted imaging distinguishes the vegetative state from the minimally conscious state. *NeuroImage, 54*(1), 103–112. http://dx.doi.org/10.1016/j.neuroimage.2010.08.035.

Fernandez-Espejo, D., Junque, C., Bernabeu, M., Roig-Rovira, T., Vendrell, P., & Mercader, J. M. (2010). Reductions of thalamic volume and regional shape changes in the vegetative and the minimally conscious states. *Journal of Neurotrauma, 27*(7), 1187–1193. http://dx.doi.org/10.1089/neu.2010.1297.

Fernandez-Espejo, D., & Owen, A. M. (2013). Detecting awareness after severe brain injury. *Nature Reviews Neuroscience, 14*(11), 801–809. http://dx.doi.org/10.1038/nrn3608.

Fernandez-Espejo, D., Soddu, A., Cruse, D., Palacios, E. M., Junque, C., Vanhaudenhuyse, A., et al. (2012). A role for the default mode network in the bases of disorders of consciousness. *Annals of Neurology, 72*(3), 335–343. http://dx.doi.org/10.1002/ana.23635.

Fridman, E. A., Beattie, B. J., Broft, A., Laureys, S., & Schiff, N. D. (2014). Regional cerebral metabolic patterns demonstrate the role of anterior forebrain mesocircuit dysfunction in the severely injured brain. *Proceedings of the National Academy of Sciences of the United States of America, 111*(17), 6473–6478. http://dx.doi.org/10.1073/pnas.1320969111.

Galanaud, D., Perlbarg, V., Gupta, R., Stevens, R. D., Sanchez, P., Tollard, E., et al. (2012). Assessment of white matter injury and outcome in severe brain trauma: A prospective multicenter cohort. *Anesthesiology, 117*(6), 1300–1310. http://dx.doi.org/10.1097/ALN.0b013e3182755558.

Giacino, J. T., Fins, J. J., Laureys, S., & Schiff, N. D. (2014). Disorders of consciousness after acquired brain injury: The state of the science. *Nature Reviews. Neurology, 10*(2), 99–114. http://dx.doi.org/10.1038/nrneurol.2013.279.

Giacino, J. T., Kalmar, K., & Whyte, J. (2004). The JFK coma recovery scale-revised: Measurement characteristics and

diagnostic utility. *Archives of Physical Medicine and Rehabilitation, 85*(12), 2020–2029.

Gong, G., Rosa-Neto, P., Carbonell, F., Chen, Z. J., He, Y., & Evans, A. C. (2009). Age- and gender-related differences in the cortical anatomical network. *The Journal of Neuroscience, 29*(50), 15684–15693. http://dx.doi.org/10.1523/JNEUROSCI.2308-09.2009.

Gosseries, O., Di, H., Laureys, S., & Boly, M. (2014). Measuring consciousness in severely damaged brains. *Annual Review of Neuroscience, 37*, 457–478. http://dx.doi.org/10.1146/annurev-neuro-062012-170339.

Haber, S. N. (2003). The primate basal ganglia: Parallel and integrative networks. *Journal of Chemical Neuroanatomy, 26*(4), 317–330. http://dx.doi.org/10.1016/j.jchemneu.2003.10.003.

Hagmann, P. (2005). *From diffusion MRI to brain connectomics.* Thesis. Lausanne: EPFL. doi:10.5075/epfl-thesis-323.

Hagmann, P., Cammoun, L., Gigandet, X., Meuli, R., Honey, C. J., Wedeen, V. J., et al. (2008). Mapping the structural core of human cerebral cortex. *Plos Biology, 6*(7), e159. http://dx.doi.org/10.1371/journal.pbio.0060159.

Ham, T. E., Bonnelle, V., Hellyer, P., Jilka, S., Robertson, I. H., Leech, R., et al. (2014). The neural basis of impaired self-awareness after traumatic brain injury. *Brain, 137*(Pt 2), 586–597. http://dx.doi.org/10.1093/brain/awt350.

van den Heuvel, M. P., & Sporns, O. (2011). Rich-club organization of the human connectome. *The Journal of Neuroscience, 31*(44), 15775–15786. http://dx.doi.org/10.1523/JNEUROSCI.3539-11.2011.

van den Heuvel, M. P., & Sporns, O. (2013). Network hubs in the human brain. *Trends in Cognitive Sciences, 17*(12), 683–696. http://dx.doi.org/10.1016/j.tics.2013.09.012.

Honey, C. J., & Sporns, O. (2008). Dynamical consequences of lesions in cortical networks. *Human Brain Mapping, 29*(7), 802–809. http://dx.doi.org/10.1002/hbm.20579.

Hulkower, M. B., Poliak, D. B., Rosenbaum, S. B., Zimmerman, M. E., & Lipton, M. L. (2013). A decade of DTI in traumatic brain injury: 10 years and 100 articles later. *AJNR (American Journal of Neuroradiology), 34*(11), 2064–2074. http://dx.doi.org/10.3174/ajnr.A3395.

Ishai, A., Ungerleider, L. G., Martin, A., & Haxby, J. V. (2000). The representation of objects in the human occipital and temporal cortex. *Journal of Cognitive Neuroscience, 12*(Suppl 2), 35–51. http://dx.doi.org/10.1162/089892900564055.

Jones, D. K., & Cercignani, M. (2010). Twenty-five pitfalls in the analysis of diffusion MRI data. *NMR in Biomedicine, 23*(7), 803–820. http://dx.doi.org/10.1002/nbm.1543.

Jones, D. K., Knosche, T. R., & Turner, R. (2013). White matter integrity, fiber count, and other fallacies: The do's and don'ts of diffusion MRI. *NeuroImage, 73*, 239–254. http://dx.doi.org/10.1016/j.neuroimage.2012.06.081.

Koch, C., Massimini, M., Boly, M., & Tononi, G. (2016a). Neural correlates of consciousness: Progress and problems. *Nature Reviews Neuroscience, 17*(5), 307–321. http://dx.doi.org/10.1038/nrn.2016.22.

Koch, C., Massimini, M., Boly, M., & Tononi, G. (2016b). Neural correlates of consciousness: Progress and problems [Review] *Nature Reviews Neuroscience, 17*(5), 307–321. http://dx.doi.org/10.1038/nrn.2016.22.

Kraus, M. F., Susmaras, T., Caughlin, B. P., Walker, C. J., Sweeney, J. A., & Little, D. M. (2007). White matter integrity and cognition in chronic traumatic brain injury: A diffusion tensor imaging study. *Brain, 130*(Pt 10), 2508–2519. http://dx.doi.org/10.1093/brain/awm216.

Lant, N. D., Gonzalez-Lara, L. E., Owen, A. M., & Fernández-Espejo, D. (2016). Relationship between the anterior forebrain mesocircuit and the default mode network in the structural bases of disorders of consciousness. *NeuroImage: Clinical, 10*, 27–35.

Laureys, S., Goldman, S., Phillips, C., Van Bogaert, P., Aerts, J., Luxen, A., et al. (1999). Impaired effective cortical connectivity in vegetative state: Preliminary investigation using PET. *NeuroImage, 9*(4), 377–382. http://dx.doi.org/10.1006/nimg.1998.0414.

Laureys, S., & Schiff, N. D. (2012). Coma and consciousness: Paradigms (re)framed by neuroimaging. *NeuroImage, 61*(2), 478–491. http://dx.doi.org/10.1016/j.neuroimage.2011.12.041.

Laureys, S., & Tononi, G. (2011). *The neurology of consciousness: Cognitive neuroscience and neuropathology.* Academic Press.

Le Bihan, D., & Johansen-Berg, H. (2012). Diffusion MRI at 25: Exploring brain tissue structure and function. *NeuroImage, 61*(2), 324–341. http://dx.doi.org/10.1016/j.neuroimage.2011.11.006.

Leemans, A., & Jones, D. K. (2009). The B-matrix must be rotated when correcting for subject motion in DTI data. *Magnetic Resonance in Medicine, 61*(6), 1336–1349. http://dx.doi.org/10.1002/mrm.21890.

Long, J., Xie, Q., Ma, Q., Urbin, M. A., Liu, L., Weng, L., et al. (2016). Distinct interactions between fronto-parietal and default mode networks in impaired consciousness. *Scientific Reports, 6*, 38866. http://dx.doi.org/10.1038/srep38866.

Lutkenhoff, E. S., Chiang, J., Tshibanda, L., Kamau, E., Kirsch, M., Pickard, J. D., et al. (2015). Thalamic and extrathalamic mechanisms of consciousness after severe brain injury. *Annals of Neurology, 78*(1), 68–76. http://dx.doi.org/10.1002/ana.24423.

Lutkenhoff, E. S., Rosenberg, M., Chiang, J., Zhang, K., Pickard, J. D., Owen, A. M., et al. (2014). Optimized brain extraction for pathological brains (optiBET). *PLos One, 9*(12), e115551. http://dx.doi.org/10.1371/journal.pone.0115551.

Luyt, C. E., Galanaud, D., Perlbarg, V., Vanhaudenhuyse, A., Stevens, R. D., Gupta, R., et al. (2012). Diffusion tensor imaging to predict long-term outcome after cardiac arrest: A bicentric pilot study. *Anesthesiology, 117*(6), 1311–1321. http://dx.doi.org/10.1097/ALN.0b013e318275148c.

MacDonald, A. A., Naci, L., MacDonald, P. A., & Owen, A. M. (2015). Anesthesia and neuroimaging: Investigating the neural correlates of unconsciousness. *Trends in Cognitive Sciences, 19*(2), 100–107. http://dx.doi.org/10.1016/j.tics.2014.12.005.

Monti, M. M., Rosenberg, M., Finoia, P., Kamau, E., Pickard, J. D., & Owen, A. M. (2015). Thalamo-frontal connectivity mediates top-down cognitive functions in disorders of consciousness. *Neurology, 84*(2), 167–173. http://dx.doi.org/10.1212/WNL.0000000000001123.

Monti, M. M., Vanhaudenhuyse, A., Coleman, M. R., Boly, M., Pickard, J. D., Tshibanda, L., et al. (2010). Willful modulation of brain activity in disorders of consciousness. *The New England Journal of Medicine, 362*(7), 579–589. http://dx.doi.org/10.1056/NEJMoa0905370.

Mori, S., Oishi, K., Jiang, H., Jiang, L., Li, X., Akhter, K., et al. (2008). Stereotaxic white matter atlas based on diffusion tensor imaging in an ICBM template. *NeuroImage, 40*(2), 570–582. http://dx.doi.org/10.1016/j.neuroimage.2007.12.035.

Owen, A. M. (2013). Detecting consciousness: A unique role for neuroimaging. *Annual Review of Psychology, 64*, 109–133. http://dx.doi.org/10.1146/annurev-psych-113011-143729.

Pencina, M. J., D'Agostino, R. B., Sr., D'Agostino, R. B., Jr., & Vasan, R. S. (2008). Evaluating the added predictive ability of a new marker: From area under the ROC curve to reclassification and beyond. *Statistics in Medicine, 27*(2), 157–172. http://dx.doi.org/10.1002/sim.2929. discussion 207-112.

Posnansky, O., Kupriyanova, Y., & Shah, N. J. (2011). On the problem of gradient calibration in diffusion weighted imaging. *International Journal of Imaging Systems and Technology, 21*(3), 271–279. http://dx.doi.org/10.1002/ima.20292.

Proix, T., Spiegler, A., Schirner, M., Rothmeier, S., Ritter, P., & Jirsa, V. K. (2016). How do parcellation size and short-range connectivity affect dynamics in large-scale brain network

models? *NeuroImage, 142*, 135–149. http://dx.doi.org/10.1016/j.neuroimage.2016.06.016.

Renier, L. A., Anurova, I., De Volder, A. G., Carlson, S., VanMeter, J., & Rauschecker, J. P. (2010). Preserved functional specialization for spatial processing in the middle occipital gyrus of the early blind. *Neuron, 68*(1), 138–148. http://dx.doi.org/10.1016/j.neuron.2010.09.021.

de Reus, M. A., & van den Heuvel, M. P. (2013). The parcellation-based connectome: Limitations and extensions. *NeuroImage, 80*, 397–404.

Ripolles, P., Marco-Pallares, J., de Diego-Balaguer, R., Miro, J., Falip, M., Juncadella, M., et al. (2012). Analysis of automated methods for spatial normalization of lesioned brains. *NeuroImage, 60*(2), 1296–1306. http://dx.doi.org/10.1016/j.neuroimage.2012.01.094.

Rubinov, M., & Sporns, O. (2010). Complex network measures of brain connectivity: Uses and interpretations. *NeuroImage, 52*(3), 1059–1069. http://dx.doi.org/10.1016/j.neuroimage.2009.10.003.

Salazar, R. F., Dotson, N. M., Bressler, S. L., & Gray, C. M. (2012). Content-specific fronto-parietal synchronization during visual working memory. *Science, 338*(6110), 1097–1100. http://dx.doi.org/10.1126/science.1224000.

Schiff, N. D. (2008). Central thalamic contributions to arousal regulation and neurological disorders of consciousness. *Annals of the New York Academy of Sciences, 1129*, 105–118. http://dx.doi.org/10.1196/annals.1417.029.

Schiff, N. D. (2010). Recovery of consciousness after brain injury: A mesocircuit hypothesis. *Trends in Neurosciences, 33*(1), 1–9. http://dx.doi.org/10.1016/j.tins.2009.11.002.

Schiff, N. D. (2016). Central thalamic deep brain stimulation to support anterior forebrain mesocircuit function in the severely injured brain. *Journal of Neural Transmission (Vienna), 123*(7), 797–806.

Schiff, N. D., & Fins, J. J. (2007). Deep brain stimulation and cognition: Moving from animal to patient. *Current Opinion in Neurology, 20*(6), 638–642. http://dx.doi.org/10.1097/WCO.0b013e3282f1c6e4.

Schiff, N. D., & Plum, F. (2000). The role of arousal and "gating" systems in the neurology of impaired consciousness. *Journal of Clinical Neurophysiology, 17*(5), 438–452.

Schurger, A., Pereira, F., Treisman, A., & Cohen, J. D. (2010). Reproducibility distinguishes conscious from nonconscious neural representations. *Science, 327*(5961), 97–99. http://dx.doi.org/10.1126/science.1180029.

Shadlen, M. N., & Kiani, R. (2011). *Consciousness as a decision to engage* characterizing Consciousness: From Cognition to the clinic? Springer.

Silva, S., de Pasquale, F., Vuillaume, C., Riu, B., Loubinoux, I., Geeraerts, T., et al. (2015). Disruption of posteromedial large-scale neural communication predicts recovery from coma. *Neurology, 85*(23), 2036–2044. http://dx.doi.org/10.1212/WNL.0000000000002196.

Song, S. K., Sun, S. W., Ju, W. K., Lin, S. J., Cross, A. H., & Neufeld, A. H. (2003). Diffusion tensor imaging detects and differentiates axon and myelin degeneration in mouse optic nerve after retinal ischemia. *NeuroImage, 20*(3), 1714–1722.

Song, S. K., Yoshino, J., Le, T. Q., Lin, S. J., Sun, S. W., Cross, A. H., et al. (2005). Demyelination increases radial diffusivity in corpus callosum of mouse brain. *NeuroImage, 26*(1), 132–140. http://dx.doi.org/10.1016/j.neuroimage.2005.01.028.

Sporns, O. (2011). The human connectome: A complex network. *Annals of the New York Academy of Sciences, 1224*, 109–125. http://dx.doi.org/10.1111/j.1749-6632.2010.05888.x.

Sporns, O., Tononi, G., & Edelman, G. M. (2000). Connectivity and complexity: The relationship between neuroanatomy and brain dynamics. *Neural Networks, 13*(8–9), 909–922.

Sporns, O., Tononi, G., & Kotter, R. (2005). The human connectome: A structural description of the human brain. *Plos Computational Biology, 1*(4), e42. http://dx.doi.org/10.1371/journal.pcbi.0010042.

Stender, J., Gosseries, O., Bruno, M. A., Charland-Verville, V., Vanhaudenhuyse, A., Demertzi, A., et al. (2014). Diagnostic precision of PET imaging and functional MRI in disorders of consciousness: A clinical validation study. *Lancet, 384*(9942), 514–522. http://dx.doi.org/10.1016/S0140-6736(14)60042-8.

Telesford, Q. K., Burdette, J. H., & Laurienti, P. J. (2013). An exploration of graph metric reproducibility in complex brain networks. *Frontiers of Neuroscience, 7*, 67. http://dx.doi.org/10.3389/fnins.2013.00067.

Wang, J., Wang, X., Xia, M., Liao, X., Evans, A., & He, Y. (2015). GRETNA: A graph theoretical network analysis toolbox for imaging connectomics. *Frontiers in Human Neuroscience, 9*, 386. http://dx.doi.org/10.3389/fnhum.2015.00386.

Wendelken, C., Ferrer, E., Whitaker, K. J., & Bunge, S. A. (2015). Fronto-parietal network reconfiguration supports the development of reasoning ability. *Cerebral Cortex*. http://dx.doi.org/10.1093/cercor/bhv050.

Wheeler-Kingshott, C. A., & Cercignani, M. (2009). About "axial" and "radial" diffusivities. *Magnetic Resonance in Medicine, 61*(5), 1255–1260. http://dx.doi.org/10.1002/mrm.21965.

Wu, X., Zou, Q., Hu, J., Tang, W., Mao, Y., Gao, L., et al. (2015). Intrinsic functional connectivity patterns predict consciousness level and recovery outcome in acquired brain injury. *The Journal of Neuroscience, 35*(37), 12932–12946. http://dx.doi.org/10.1523/JNEUROSCI.0415-15.2015.

Yendiki, A., Koldewyn, K., Kakunoori, S., Kanwisher, N., & Fischl, B. (2013). Spurious group differences due to head motion in a diffusion MRI study. *NeuroImage, 88C*, 79–90. http://dx.doi.org/10.1016/j.neuroimage.2013.11.027.

Zalesky, A., Fornito, A., & Bullmore, E. T. (2010). Network-based statistic: Identifying differences in brain networks. *NeuroImage, 53*(4), 1197–1207. http://dx.doi.org/10.1016/j.neuroimage.2010.06.041.

Zalesky, A., Fornito, A., Harding, I. H., Cocchi, L., Yücel, M., Pantelis, C., et al. (2010). Whole-brain anatomical networks: Does the choice of nodes matter? *NeuroImage, 50*(3), 970–983.

Zanto, T. P., & Gazzaley, A. (2013). Fronto-parietal network: Flexible hub of cognitive control. *Trends in Cognitive Sciences, 17*(12), 602–603. http://dx.doi.org/10.1016/j.tics.2013.10.001.

Zhang, R., Wei, Q., Kang, Z., Zalesky, A., Li, M., Xu, Y., et al. (2015). Disrupted brain anatomical connectivity in medication-naive patients with first-episode schizophrenia. *Brain Structure & Function, 220*(2), 1145–1159. http://dx.doi.org/10.1007/s00429-014-0706-z.

Zheng, Z. S., Reggente, N., Lutkenhoff, E., Owen, A. M., & Monti, M. M. (2017). Disentangling disorders of consciousness: Insights from diffusion tensor imaging and machine learning. *Human Brain Mapping, 38*(1), 431–443. http://dx.doi.org/10.1002/hbm.23370.

Zhong, S., He, Y., & Gong, G. (2015). Convergence and divergence across construction methods for human brain white matter networks: An assessment based on individual differences. *Human Brain Mapping, 36*(5), 1995–2013. http://dx.doi.org/10.1002/hbm.22751.